Opto-Electronic Advances

Article

February 2024, Vol. 7, No. 2

DOI: 10.29026/oea.2024.230072

Generation of lossy mode resonances (LMR) using perovskite nanofilms

Dayron Armas[1], Ignacio R. Matias[1,2]*, M. Carmen Lopez-Gonzalez[3], Carlos Ruiz Zamarreño[1,2], Pablo Zubiate[1], Ignacio del Villar[1,2] and Beatriz Romero[3]

The results presented here show for the first time the experimental demonstration of the fabrication of lossy mode resonance (LMR) devices based on perovskite coatings deposited on planar waveguides. Perovskite thin films have been obtained by means of the spin coating technique and their presence was confirmed by ellipsometry, scanning electron microscopy, and X-ray diffraction testing. The LMRs can be generated in a wide wavelength range and the experimental results agree with the theoretical simulations. Overall, this study highlights the potential of perovskite thin films for the development of novel LMR-based devices that can be used for environmental monitoring, industrial sensing, and gas detection, among other applications.

Keywords: perovskite; thin films; slab waveguide; lossy mode resonance

Armas D, Matias IR, Lopez-Gonzalez MC et al. Generation of lossy mode resonances (LMR) using perovskite nanofilms. *Opto-Electron Adv* **7**, 230072 (2024).

Introduction

Lossy mode resonance (LMR) is an optical phenomenon that has attracted great research efforts in the field of sensing applications[1]. It has many benefits over previously explored and commercially exploited sensors like those based on localized surface plasmon resonances (LSPR) or long-period fiber gratings (LPFG), for example. Among those advantages, LMR based sensors permit to achieve very high sensitivities, more than 14000 nm per refractive index unit (nm/RIU) if the surrounding medium is water[2] and more than 1000000 nm/RIU if the surrounding medium approaches the refractive index of silica, around 1.45[3]. In addition, unlike surface plasmon resonances (SPR), LMR can be observed for both Transversal Electric (TE) and Transversal Magnetic (TM) polarization modes, and if the coating thickness is properly adjusted, the LMR position can be tuned and also several resonances can be observed in the spectrum[4].

The key in order to generate an LMR is to choose the material for the thin film properly. In this sense, the material must satisfy the following conditions: the real part of the permittivity thin film has to be positive and higher in magnitude than its own imaginary part and higher than the real part of the permittivity of both the optical waveguide and the external medium surrounding the thin film[1]. Many materials have already been studied in order to obtain LMR devices, that include, metal oxides

[1]Electrical, Electronic and Communications Engineering Department, Public University of Navarra, Pamplona 31006, Spain; [2]Institute of Smart Cities (ISC), Public University of Navarra, Pamplona 31006, Spain; [3]Experimental Science and Technology School, Rey Juan Carlos University, Mostoles 28933, Spain.

*Correspondence: IR Matias, E-mail: natxo@unavarra.es

Received: 5 May 2023; Accepted: 29 August 2023; Published online: 19 December 2023

such as, tin oxide[5], zinc oxide[6], titanium oxide[7], indium-tin oxide[8], aluminum-zinc oxide (AZO)[9], indium-gallium-zinc oxide (IGZO)[10] or hafnium and tantalum[11], polymers such as poly(acrylic acid) (PAA) and poly(allylamine hydrochloride) (PAH)[12] or silicon nitride[13]. Each of these materials can change its properties in the presence of different physical and chemical parameters, such as humidity[14], volatile organic compounds[15], etc., and therefore, it is possible to design sensors based on LMRs for different applications.

The operating principle of LMR-based devices is the following: LMR will suffer a wavelength shift if either a variation in the properties of the LMR support film (either refractive index or thickness) or a change in the optical properties (refractive index) of the surrounding media occurs[1]. In this sense, the number of applications for sensors based on LMR continues to grow and includes detection of refractive index, pH, temperature, chemical composition, bending, strain, voltage, and volatile organic compounds[1]. Moreover, platforms based on LMRs can be used as chemical sensors and biosensors with significant improvements in detection limits over preceding technologies, such as 0.01 mg/mL of avidin protein[16], 150 ng/mL of immunoglobulin G[17] or 100 ng/mL of D-dimer antigen[18]. Some research is also being conducted dedicated to multiparameter sensing applications using multiple coatings in the same sensor[19,20].

However, further research is needed on materials that allow the generation of new LMR-based devices. Here, it is important to note that both the real part of the refractive index and the dispersion of the material are critical for the sensitivity of the device, while the imaginary part of the refractive index rules the depth of the LMR[21,22], and deep resonances permit to accurately monitor the LMR shift. Finally, it is also important to remark that the utilization of new materials that present adequate conditions for the generation of LMRs at longer wavelengths would permit to achieve higher sensitivities.

In this work we focus on the perovskite as novel LMR-supporting thin film material. Perovskites have already been studied for generating LMR but just in theoretical cases[23,24]. Perovskites are a family of materials with outstanding optical and electrical properties that have been extensively used as the active layer of LEDs[25], photodetectors[26], including X ray photodetectors[27], sensors[28], and photovoltaic solar cells[29].

This report presents the first experimental generation of LMRs based on mixed-cation mixed-halide perovskite thin films. The experimental results are further supported by theoretical simulations.

Experimental section

Fabrication of perovskite film

Samples were fabricated on soda lime silica glass substrates from Sigma-Aldrich with dimensions of 18×18×0.15 mm and optical properties found in ref.[30]. Along with these, other samples were fabricated on single side polished silicon wafer substrates from Sigma-Aldrich with 76.2 mm of diameter and 0.5 mm of thickness. The former were utilized for the spectrometry analysis of the transmitted light, and the latter for the ellipsometry, scanning electron microscopy (SEM) and X-ray diffraction (XRD) tests. Prior to fabrication, substrates were brushed with Hellmanex solution in water (2:98 %V) and rinsed with deionized water. After that, they were sequentially cleaned in consecutive ultrasonic baths for 15 minutes with Hellmanex solution, deionized water, isopropanol, and acetone. Finally, the substrates were dried with a nitrogen flow. Next, they were treated with UV/O_3 for 15 minutes using an Ozone Cleaner. Once the substrates were cleaned, a thin layer of PEDOT:PSS was spin-coated on top at 3000 rpm for 30 s followed by annealing at 120 °C for 10 min and then transferred into a nitrogen glovebox (O_2 and H_2O levels below 0.5 ppm).

Thin perovskite films have been fabricated with different molar precursor concentrations, i.e. 0.4 M, 0.8 M and 1.5 M (concentration relative to the DMSO:DMF (dimethyl sulfoxide and N,N-dimethylformamide)) based on mixed-cation lead mixed-halide perovskite. In particular, the perovskite is composed of formamidinium lead triiodide ($FAPbI_3$) and methylammonium lead tribromide ($MAPbBr_3$) solutions (5:1%V, respectively) both in 1:4%V DMSO:DMF, to which it was added 5%V of cesium iodide (CsI) solution in DMSO and 5%V of rubidium ioidide (RbI) solution in 1:4%V DMSO:DMF.

The perovskite film ($Cs_{0.05}Rb_{0.05}(MA_{0.17}FA_{0.83})_{0.9}Pb(I_{0.83}Br_{0.17})_3$) was deposited by spin-coating on top of the PEDOT:PSS layer using a two-step program: 1) 1000 rpm, 10 s; 2) 6000 rpm, 20 s. During the second step, chlorobenzene was added as antisolvent on the spinning substrate 5 s before the sample stopped. After that, the samples were annealed at 100 °C for 60 min using a hot plate.

Experimental setup

Figure 1 illustrates the experimental setup used to characterize the device. It consisted of a broadband white light source with a multimode optical fiber pigtail connected at its output. The cleaved end of the pigtail is positioned in front of one lateral side of the coverslip for a microscope glass slide, which acts as a planar waveguide. The perovskite coating is applied to one of the two faces of the coverslip. The output light leaves the coverslip and passes through a polarizer. Afterwards, it is collected by a multimode optical fiber pigtail. The other end of the multimode optical fiber pigtail is connected to a spectrometer.

A multimode optical fiber (FT200EMT with 200/225 μm core/cladding diameter) was purchased from ThorLabs and used to prepare the pigtails that transport the optical signal. Broadband white light source (Takhi-HP halogen) was obtained from Pyroistech. Two spectrometers (USB2000 and Nirquest with wavelength ranges from 400 nm to 1000 nm and from 900 nm to 1700 nm respectively), from Ocean Insight were used to monitor the spectral responses of the devices. Two different polarizers, both from ThorLabs, were used to filter the wide spectral range, one for the visible and the other for the near-infrared ranges, and allowed to separate Transversal Electric (TE) and Transversal Magnetic (TM) light polarization modes.

Ellipsometry, SEM and XRD analysis

A scanning electron microscopy (SEM), model UltraPlus FESEM from Carl Zeiss Inc, with an in-lens detector at 3 kV and an aperture diameter of 30 μm, was used to carry out thickness measurements of perovskites on the coverslips samples.

In addition, an X-ray diffraction (XRD) tool was used to determine the chemical elements present in a film of perovskite coated onto glass substrate. The measurements were performed with PANalytical model X'Pert PRO MRD PANalytical diffractometer operating at 45 kV and 40 mA, employing Cu K_α radiation with a secondary monochromator to filter K_β and a sealed Xenon point detector. A step size of 0.04° and 2 seconds per step was employed in a range of 10°–100°.

The elliposemetry measurement was used to determine the refractive index of the material. The chart was obtained by using an ellipsometer UVISEL, with spectral range of 0.6–6.5 eV (190–2100 nm), an angle of incidence of 70°, a spot size of 1 mm, and software DeltaPsi2TM (from Horiba Scientific Thin Film Division) were used. All these values, specifically the thickness and index of the material, were used to carry out the simulations

Theoretical analysis

For the theoretical analysis of the experimental setup of Fig. 1, after the deposition of the perovskite film, the optical response was estimated by a means of a numerical software calculations based on the well-known plane wave method for a one-dimensional multilayer waveguide[31], validated for both SPR[32] and LMR[4]. The refractive index of the coverslip was calculated for every wavelength using the dispersion formula (1) of the soda lime glass[30]:

$$n = 1.5130 + 0.003169\lambda^2 + 0.003962\lambda^{-2}\,. \qquad (1)$$

The refractive index of the perovskite coating used for the analysis was obtained by performing ellipsometry

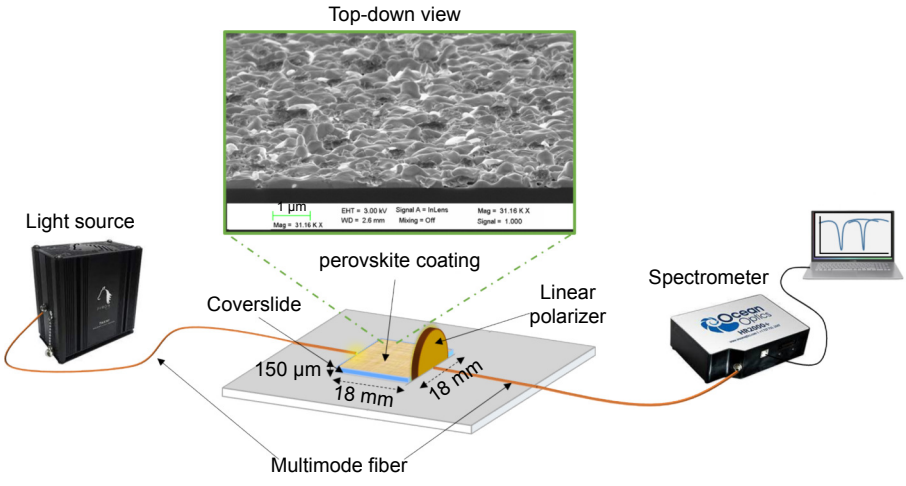

Fig. 1 | Experimental setup used to characterize the sample and cross-section detail of perovskite coating on the coverslips.

(UVISEL 2 from Horiba) to a sample deposited onto a slice of silicon wafer (see Results section).

Results and discussion

The impact of the proposed perovskite film was analyzed from a theoretical and experimental point of view. In this sense, and to carry out a complete study, three sensors with three different thicknesses of perovskites were manufactured. For that, the film deposited on the coverslips carefully analyzed by means of SEM imaging, together with X-EDS, thus obtaining the thickness and the chemical elements present of the deposited perovskites. In addition, for the development of the simulations it is also necessary to know the refractive index (n) and the extinction coefficient (k). Consequently, ellipsometry measurements were also carried out.

Figure 2 shows three SEM images of the cross-section corresponding to three different samples coated with three different perovskites thickness. Here, it is important to note that the film thickness was measured from several images on different portion of the samples in order to calculate the mean thickness and the standard deviation for each sample. In the case of the first sample, as can be seen in Fig. 2(a), the mean value of the perovskites thickness was 114±33 nm. Regarding the second sample, as shown in Fig. 2(b), the measured thickness of the film was 276±19 nm. Lastly, in the case of the third sample, as seen in Fig. 2(c), the thickness obtained was 648±41 nm.

XRD analysis was performed on the samples in order to determinate the crystal structure of the perovskite thin films. The XRD spectrum (Fig. 2(d)) clearly shows the characteristic peaks of a stable perovskite film located at 14.09° (001), 19.91° (011), 24.59° (111), 28.41° (002),

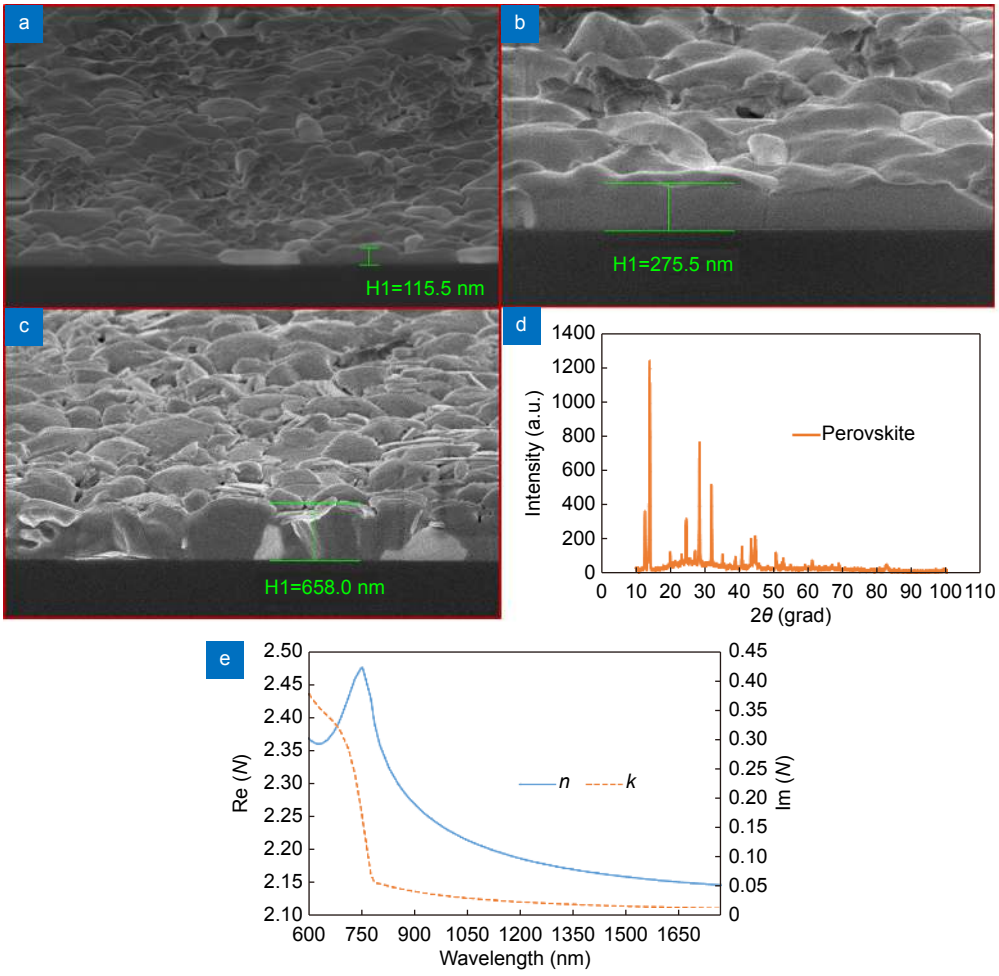

Fig. 2 | SEM image of the cross section of a coverslips coated with perovskite film: (**a**) The mean value of the thickness measured on different portions from sample was 114 nm. (**b**) The mean value of the thickness of the sample 2 was 276 nm. (**c**) The mean value of the thickness of the sample 3 was 648 nm. (**d**) XRD pattern of perovskite. (**e**) Complex refractive index real part (Re N or n) and imaginary part of extinction coefficient (Im N or k) of perovskite obtained from spectroscopic ellipsometry.

31.86° (012), 35.04° (112), 40.69° (022), 43.31° (003) and 50.43° (222). No database has been used to identify the main peaks observed in XRD spectrum since this fourcation two-halide PVK is a new composition, and there is no database available. However, the main peaks observed in the spectrum match the standard peaks in MAPI and CsFAPbIBr[33–35]. Additional peaks appearing in the spectrum require a more detailed analysis to be identify, which is beyond the scope of this work.

Figure 2(e) shows the dispersion curves of the refractive index RI (n) and the extinction coefficient (k) of perovskites films as a function of the wavelength obtained using an ellipsometer, where the refractive index and extinction coefficient meet the requirements for LMR generation in all the studied wavelength range.

One of the typical characteristics of LMR is that the position of the resonance can be easily tuned along the optical spectrum by changing the thin film thickness. In addition, while increasing the thickness of the thin film, higher order resonances emerge[1]. In order to analyze and demonstrate experimentally the perovskites as LMR supporting coating, the three devices were characterized using the setup of Fig. 1. The transmission spectra were recorded both at TE and TM polarization in a wavelength range covering from 750 nm to 1700 nm of the optical spectrum.

Regarding the sensing platform, LMRs can be generated with both planar configuration and optical fiber. Here, planar configuration is preferred instead of optical fiber due to several advantages, such as an easy-to-handle and cost-effective setup that avoids the need for optical fiber splices. Moreover, the planar configuration enables to control the polarization with a linear polarizer instead of more complex setups used in optical fiber where a polarizer controller and an in-line-polarizer are required and where it is also necessary to readjust the system each time a new experiment is performed[7].

The transmission spectra of a theoretical perovskite coated sample were calculated by the plane wave method for a one-dimensional multilayer waveguide[21,31], for the wavelength range from 750 nm to 1700 nm and for a coating thickness range from 85 nm to 650 nm. These results are shown in Fig. 3 using a heat map where darker blue areas represent the deepest attenuation of the spectrum, corresponding to LMR central wavelengths. Therefore, Fig. 3 shows the evolution of the LMR transmission as a function of the coating thickness deposited onto the planar waveguides. Here, it is possible to identify three LMR. In fact, from Fig. 3 it can be observed a first transmission minimum for an approximate thickness of 50 nm, which corresponds to the first LMR. In addition, first LMR experience a shift to long wavelengths when the coating thickness is increased. Under the same argument, it can be observed that the second LMR starts to be visible for thickness 235 nm and the third LMR for thickness 430 nm.

As can be seen in Fig. 3, the three fabricated samples are represented by vertical dotted lines, while the central wavelengths of the experimentally obtained LMRs are indicated by red circles. Overall, the experimental LMRs demonstrate good agreement with the calculated LMRs for the same coating thickness, with a minor shift observed towards longer wavelengths in the experimental data.

Subsequently, a detailed analysis was performed on the three fabricated samples to compare the calculated and experimental spectra individually (see Fig. 4). Figure 4(a) illustrates the numerical and experimental spectra

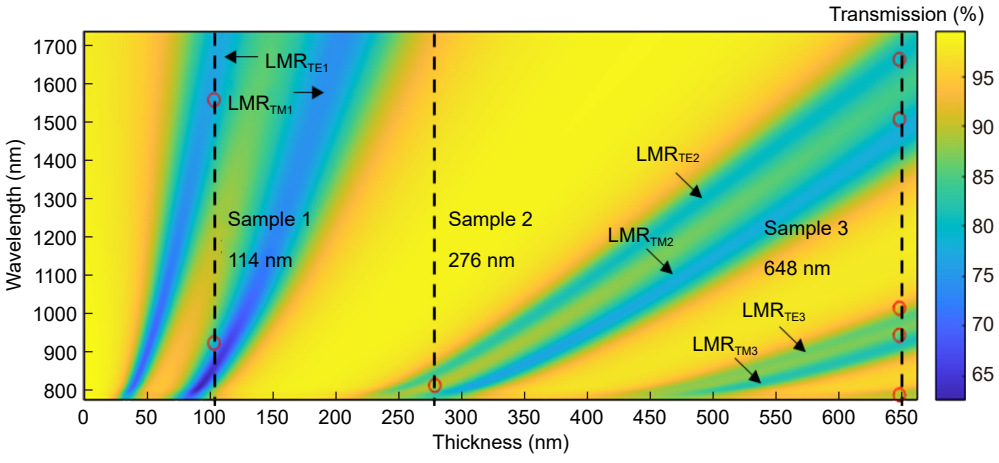

Fig. 3 | Evolution of calculated LMRs in the transmission spectrums vs. coating thickness and overlay of the experimental LMRs minimums.

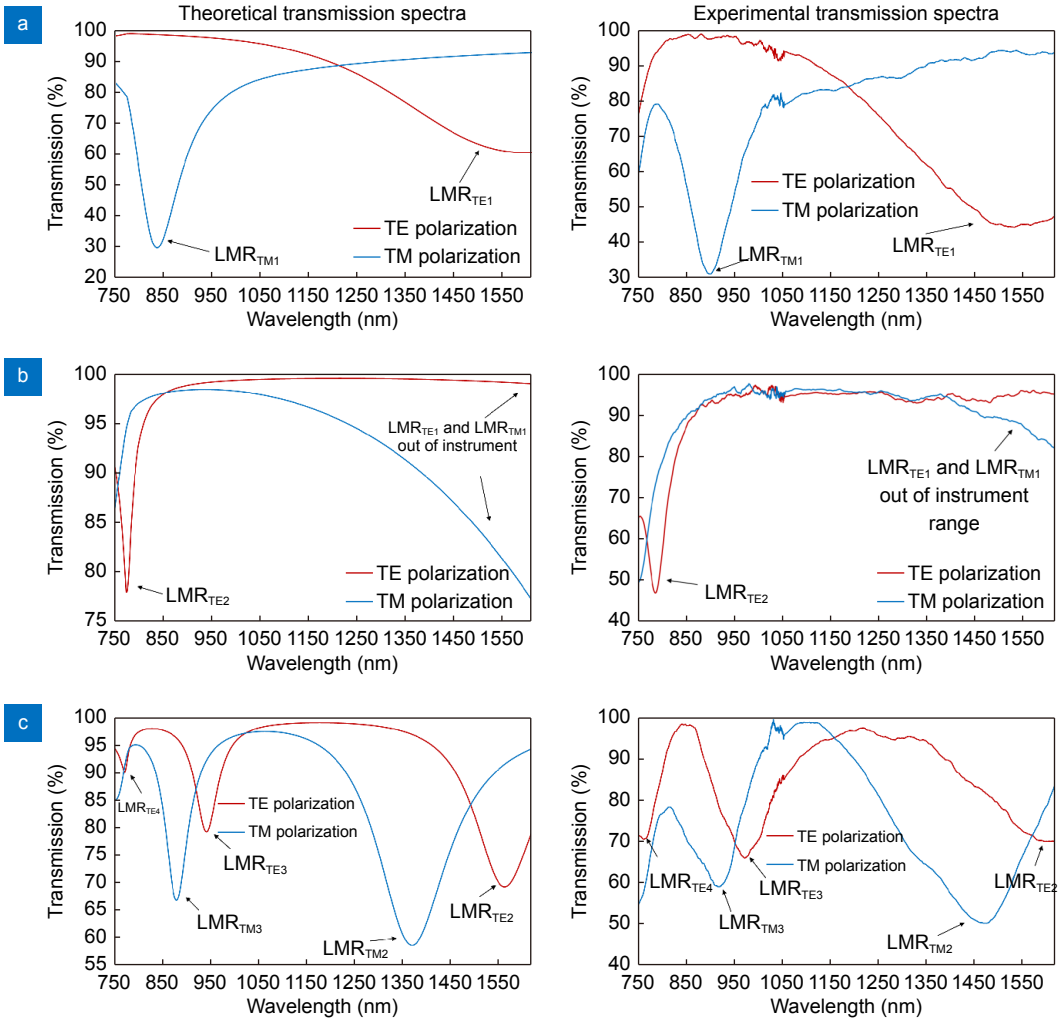

Fig. 4 | Theoretical and experimental transmission spectra of perovskite thin films with different thicknesses on planar waveguides: (**a**) 114 nm, (**b**) 276 nm, (**c**) 648 nm.

obtained from the first device, which exhibits two distinct resonances. It has been previously demonstrated that the TE polarization resonance (LMR_{TE}) is always followed by the TM polarization resonance (LMR_{TM})[21]. Therefore, it is possible to associate the longer wavelength resonance with the first order TE resonance (LMR_{TE1}) and the shorter wavelength resonance with the first order TM resonance (LMR_{TM1}).

Figure 4(b) illustrates the numerical and experimental spectra obtained for the 276 nm perovskite coating thickness. In this case, the first order LMR falls outside the detection range of the optical spectrum analyzer, while the second order LMR becomes visible. Specifically, a well-defined resonance can be observed, which corresponds to the second order resonance generated by TE polarization (LMR_{TE2}). Additionally, an initial emergence of a resonance associated with TM polarized light can be observed at the left side of the spectrum.

The final device consisted of a 648 nm perovskite coating, and its numerical and experimental spectra are shown in Fig. 4(c). This device exhibits five resonances: the longer wavelength resonances correspond to the second order TE and TM resonances (LMR_{TE2} and LMR_{TM2}), and the shorter wavelength resonances correspond to the third order resonances (LMR_{TE3} and LMR_{TM3}). Additionally, a clear resonance corresponding to the fourth order TE resonance (LMR_{TE4}) is observed at 765 nm. However, the fourth order resonance associated with TM polarization (LMR_{TM4}) falls outside the wavelength range that was monitored in this experiment.

The separation between LMR_{TE} and LMR_{TM}, as well as the difference in spectral widths of different-order LMRs, are crucial parameters to consider in understanding the behavior of LMRs. Previous studies have shown that with higher-order resonances, the separation between LMR_{TE} and LMR_{TM}, as well as the spectral

widths, decrease. This trend is also observed in our results. As shown in Fig. 4(a), the separation between LMR_{TE1} and LMR_{TM1} for the first-order resonance is 630 nm. For the second and third-order LMRs, as presented in Fig. 4(c), the separation between LMR_{TE} and LMR_{TM} is 217 nm and 72 nm, respectively. This characteristic is closely related to the progressive reduction in sensitivity observed for higher-order LMRs. Our analysis of the spectral response of the devices confirms the reduction in spectral width for higher-order resonances, supporting the unique nature of LMRs in both fiber optics and planar waveguides[36].

Conclusions

This study represents a significant step forward in the development of novel devices based on LMR, by demonstrating the feasibility of using perovskite thin films as active materials. The experimental observation of LMRs based on perovskites in a planar configuration opens up new possibilities for the design of compact and versatile photonic devices. Moreover, the variation in thicknesses of the perovskite thin films plays a significant role in shaping the optical characteristics of the developed devices. As the thickness increases, we observed a transition from lower-order to higher-order LMRs in the transmission spectra. Additionally, the spectral widths of the LMRs showed a trend of decreasing with higher-order resonances. These variations in thickness directly impact the resonance wavelengths and spectral properties of the devices, highlighting the importance of carefully controlling and optimizing the thickness of the perovskite coatings for tailored LMR-based applications. Furthermore, the use of a polarizer in conjunction with the planar configuration has allowed us to separate the TE and TM polarization modes, leading to resonances with a reduced spectral width.

In conclusion, this work provides new insights into the potential of perovskite thin films for use in the development of novel LMR devices with important sensing properties. The findings presented here open up opportunities for the application of perovskite-based LMRs in a wide range of optical sensors for environmental monitoring, industrial sensing, and gas detection, among other areas. These results may have significant implications for the development of future generations of optical sensors and pave the way for further research on the use of perovskite materials in the development of advanced optical sensors.

References

1. Del Villar I, Arregui FJ, Zamarreño CR et al. Optical sensors based on lossy-mode resonances. *Sens Actuators B Chem* **240**, 174–185 (2017).
2. Arregui FJ, Del Villar I, Zamarreño CR et al. Giant sensitivity of optical fiber sensors by means of lossy mode resonance. *Sens Actuators B Chem* **232**, 660–665 (2016).
3. Ozcariz A, Zamarreño CR, Zubiate P et al. Is there a frontier in sensitivity with lossy mode resonance (LMR) based refractometers. *Sci Rep* **7**, 10280 (2017).
4. Del Villar I, Zamarreño CR, Hernaez M et al. Lossy mode resonance generation with indium-tin-oxide-coated optical fibers for sensing applications. *J Lightwave Technol* **28**, 111–117 (2010).
5. Zubiate P, Zamarreño CR, Del Villar I et al. High sensitive refractometers based on lossy mode resonances (LMRs) supported by ITO coated D-shaped optical fibers. *Opt Express* **23**, 8045–8050 (2015).
6. Usha SP, Gupta BD. Performance analysis of zinc oxide-implemented lossy mode resonance-based optical fiber refractive index sensor utilizing thin film/nanostructure. *Appl Opt* **56**, 5716–5725 (2017).
7. Benítez M, Zubiate P, Del Villar I et al. Lossy mode resonance based microfluidic platform developed on planar waveguide for biosensing applications. *Biosensors* **12**, 403 (2022).
8. Del Villar I, Zamarreño CR, Sanchez P et al. Generation of lossy mode resonances by deposition of high-refractive-index coatings on uncladded multimode optical fibers. *J Opt* **12**, 095503 (2010).
9. Ozcariz A, Piña-Azamar D A, Zamarreño CR et al. Aluminum doped zinc oxide (AZO) coated optical fiber LMR refractometers—an experimental demonstration. *Sens Actuators B Chem* **281**, 698–704 (2019).
10. Ozcariz A, Dominik M, Smietana M et al. Lossy mode resonance optical sensors based on indium-gallium-zinc oxide thin film. *Sens Actuators A Phys* **290**, 20–27 (2019).
11. Kosiel K, Koba M, Masiewicz M et al. Tailoring properties of lossy-mode resonance optical fiber sensors with atomic layer deposition technique. *Opt Laser Technol* **102**, 213–221 (2018).
12. Zubiate P, Zamarreño CR, Del Villar I et al. D-shape optical fiber pH sensor based on lossy mode resonances (LMRs). In *2015 IEEE SENSORS* 1–4 (IEEE, 2015);http://doi.org/10.1109/ICSENS.2015.7370421.
13. Sudas DP, Zakharov LY, Jitov VA et al. Silicon oxynitride thin film coating to lossy mode resonance fiber-optic refractometer. *Sensors* **22**, 3665 (2022).
14. Bohorquez DL, Del Villar I, Corres JM et al. Generation of lossy mode resonances in a broadband range with multilayer coated coverslips optimized for humidity sensing. *Sens Actuators B Chem* **325**, 128795 (2020).
15. Elosua C, Arregui FJ, Zamarreño CR et al. Volatile organic compounds optical fiber sensor based on lossy mode resonances. *Sens Actuators B Chem* **173**, 523–529 (2012).
16. Śmietana M, Koba M, Sezemsky P et al. Simultaneous optical and electrochemical label-free biosensing with ITO-coated lossy-mode resonance sensor. *Biosens Bioelectron* **154**, 112050 (2020).
17. Chiavaioli F, Zubiate P, Del Villar I et al. Femtomolar detection by nanocoated fiber label-free biosensors. *ACS Sens* **3**, 936–943 (2018).

18. Zubiate P, Urrutia A, Zamarreño CR et al. Fiber-based early diagnosis of venous thromboembolic disease by label-free D-dimer detection. *Biosens Bioelectron X* **2**, 100026 (2019).
19. Dominguez I, Del Villar I, Fuentes O et al. Interdigital concept in photonic sensors based on an array of lossy mode resonances. *Sci Rep* **11**, 13228 (2021).
20. Dominguez I, Del Villar I, Fuentes O et al. Dually nanocoated planar waveguides towards multi-parameter sensing. *Sci Rep* **11**, 3669 (2021).
21. Del Villar I, Hernaez M, Zamarreño CR et al. Design rules for lossy mode resonance based sensors. *Appl Opt* **51**, 4298–4307 (2012).
22. Zhao WM, Wang Q. Analytical solutions to fundamental questions for lossy mode resonance. *Laser Photon Rev* **17**, 2200554 (2023).
23. Wu LM, Xiang YJ, Qin YW. Lossy-mode-resonance sensor based on perovskite nanomaterial with high sensitivity. *Opt Express* **29**, 17602–17612 (2021).
24. Yadollahzadeh S, Aghbolaghi R, Parvizi R. Perovskite-based lossy-mode resonance sensor in visible light spectrum: comparison and optimization of optical enhancements. *Phys B Condens Matter* **640**, 414048 (2022).
25. Fakharuddin A, Gangishetty MK, Abdi-Jalebi M et al. Perovskite light-emitting diodes. *Nat Electron* **5**, 203–216 (2022).
26. Li CL, Wang HL, Wang F et al. Ultrafast and broadband photodetectors based on a perovskite/organic bulk heterojunction for large-dynamic-range imaging. *Light Sci Appl* **9**, 31 (2020).
27. Deumel S, Van Breemen A, Gelinck G et al. High-sensitivity high-resolution X-ray imaging with soft-sintered metal halide perovskites. *Nat Electron* **4**, 681–688 (2021).
28. Xu W, Li FM, Cai ZX et al. An ultrasensitive and reversible fluorescence sensor of humidity using perovskite $CH_3NH_3PbBr_3$. *J Mater Chem C* **4**, 9651–9655 (2016).
29. Green MA, Ho-Baillie A, Snaith HJ. The emergence of perovskite solar cells. *Nat Photonics* **8**, 506–514 (2014).
30. Rubin M. Optical properties of soda lime silica glasses. *Sol Energy Mater* **12**, 275–288 (1985).
31. Yeh P, Yariv A, Hong CS. Electromagnetic propagation in periodic stratified media. I. General theory. *J Opt Soc Am* **67**, 423–438 (1977).
32. Sharma AK, Gupta BD. On the sensitivity and signal to noise ratio of a step-index fiber optic surface plasmon resonance sensor with bimetallic layers. *Opt Commun* **245**, 159–169 (2005).
33. da Silva Filho JMC, Marques FC. Growth of perovskite nanorods from PbS quantum dots. *MRS Adv* **3**, 1843–1848 (2018).
34. Wu KW, Bera A, Ma C et al. Temperature-dependent excitonic photoluminescence of hybrid organometal halide perovskite films. *Phys Chem Chem Phys* **16**, 22476–22481 (2014).
35. Gil-Escrig L, Momblona C, La-Placa MG et al. Vacuum deposited triple-cation mixed-halide perovskite solar cells. *Adv Energy Mater* **8**, 1703506 (2018).
36. Del Villar I, Zamarreño CR, Hernaez M et al. Generation of lossy mode resonances with absorbing thin-films. *J Lightwave Technol* **28**, 3351–3357 (2010).

Acknowledgements

The authors would like to acknowledge the partial support to Agencia Estatal de Investigación PID2019-106231RB-I00 research project, Universidad Rey Juan Carlos with research project "Células fotovoltaicas de tercera generación basadas en semiconductores orgánicos avanzados perovskitas híbridas en estructuras multiunión" (reference M2607), and the pre-doctoral research grant of the Public University of Navarra.

Author contributions

C. R. Zamarreño, I. R. Matias, and B. Romero conceived the project. D. Armas and P. Zubiate characterized properties of sensors and performed the experiments. M. C. Lopez-Gonzalez and B. Romero prepared all the chemicals and fabrication of perovskite film. D. Armas and I. D. Villar conceived the theoretical analysis and performed the simulations. C. R. Zamarreño, I. R. Matias, and B. Romero supervised the project. D. Armas, P. Zubiate, I. D. Villar and B. Romero wrote the manuscript.

Competing interests

The authors declare no competing financial interests.